RESEARCH/REVIEW ARTICLE

High-resolution electrical resistivity tomography applied to patterned ground, Wedel Jarlsberg Land, south-west Spitsbergen

Marek Kasprzak

Institute of Geography and Regional Development, University of Wrocław, pl. Uniwersytecki 1, PL-50-137 Wrocław, Poland

Keywords
Patterned ground; permafrost; active layer; electrical imaging; Svalbard.

Correspondence
Marek Kasprzak, Institute of Geography and Regional Development, University of Wrocław, pl. Uniwersytecki 1, PL-50-137 Wrocław, Poland.
E-mail: marek.kasprzak@uwr.edu.pl

Abstract

This article presents results of two-dimensional electrical resistivity tomography (ERT) applied to three types of patterned ground in Wedel-Jarlsberg Land (Svalbard), carried out in late July 2012. The structures investigated include sorted circles, non-sorted polygons and a net with sorted coarser material. ERT was used to recognize the internal ground structure, the shape of permafrost table below the active layer and the geometric relationships between permafrost, ground layering and surface patterns. Results of inversion modelling indicate that the permafrost table occurs at a depth of 0.5–1 m in a mountain valley and 1–2.5 m on raised marine terraces. The permafrost table was nearly planar beneath non-sorted deposits and wavy beneath sorted materials. The mutual relationships between the permafrost table and the shape of a stone circle are different from those typically presented in literature. Ground structure beneath the net with sorted coarser materials is complex as implied in convective models. In non-sorted polygons, the imaging failed to reveal vertical structures between them.

Patterned ground, found in different climatic zones, is most readily associated with the periglacial morphogenetic domain and the action of frost processes such as cracking due to thermal contraction, seasonal frost and desiccation (Washburn 1956). These processes are favoured in ice-free areas of high latitudes and in high mountains. Relict patterned ground and related structures, inherited from periods of Pleistocene cooling, are more widespread and widely identified in lowland terrains of Eurasia and North America (e.g., Sekyra 1956; Kaatz 1959; Williams 1964; Christensen 1974; Boardman 1987; Lusch et al. 2009; Dąbski 2011). Early reviews of patterned ground formation (Jahn 1948; Troll 1958) indicate that the origin, distribution and controls on the development of these structures generated interest as early as in the beginning of the 20th century. Among existing publications, attempts to classify patterned ground are important. They are based on morphological and less often, genetic criteria (Washburn 1956, 1969, 1970, 1979; Drew & Tedrow 1962; Tedrow 1962; Jahn 1975; Tedrow 1977). Washburn classified various types of patterned ground such as circles, polygons, nets, steps and stripes, each occurring in a sorted and non-sorted variant. In addition, there are structures that do not easily fall into any of these categories (Kessler & Werner 2003). In geomorphological works focused on internal structures of ground (e.g., Overduin & Kane 2006; Watanabe et al. 2012) or ecological research focused on vegetation succession, terms such as frost-boil and mud boil are popular, but their use should be limited to small patches of barren or sparsely vegetated soil, shaped by frost processes without the contributing role of sorting (Walker et al. 2004; van Everdingen 2005).

After more than 100 years of research, it is evident that the specific morphology of patterned ground is an outcome of various processes acting in combination. However, views diverge regarding the dominant morphogenetic factor (e.g., Jahn 1968; Goudie 2004; Schaetzl & Anderson 2005; Ballantyne 2007). Three groups of theories seem to prevail (Ballantyne 2007), in which sorting by (i) differential frost heave (e.g., Ballantyne & Matthews 1982, 1983; Kling 1997; Matsuoka et al. 2003;

Citation: *Polar Research* 2015, *34*, 25678, http://dx.doi.org/10.3402/polar.v34.25678

Peterson & Krantz 2008); (ii) buoyancy-driven soil circulation (e.g., Ray et al. 1983; Hallet & Prestrud 1986; Hallet 1998, 2013) and (iii) free convection of soil porewater during thaw (e.g., Krantz 1990) are emphasized.

To understand the mechanisms responsible for the origin of patterned ground, one needs to know their internal structures. Since obtaining insights into these structures is not straightforward, usually singular examples are investigated. Despite voluminous literature, trenches across patterned ground, particularly in coarse materials, are seldom presented (Washburn 1969; Schunke 1975). Therefore, the main aim of this article is to provide data about the internal architecture of selected types of patterned ground, such as sorted circles, non-sorted polygons and nets with coarser sorted materials, as well as to decipher the relationships between ground structure and the geometry of the permafrost table. The research reported in this article was carried out on the western coast of Spitsbergen, where these surface features are widely distributed. The specific sites subject to investigation are those described by Jahn (1975) and observed by him in 1957 and 1974.

The technique adopted was two-dimensional, high-resolution electrical resistivity tomography (2-D ERT), a non-invasive method that yields information about the variability of ground conditions along specific profiles. The resultant cross-sections reveal ground compartments, which differ in terms of geoelectric properties. So far, electrical imaging providing this degree of detail of patterned ground structure has been presented very rarely, usually in relation to the permafrost in general and land surface dominated by polygonal features (e.g., Hubbard et al. 2013). The method employed in the study is suitable for waterlogged ground, built of coarse material, where trenching would be tough and ineffective. In addition, the use of geophysics was in keeping with nature conservation principles in the Sør-Spitsbergen National Park, where the study sites were located. The results of ERT profiling were compared with idealized, "model" cross-sections of patterned ground.

Study area

The study area is located in the Wedel Jarlsberg Land, in the south-western coastal zone of Spitsbergen, ca. 15 km north–north-east from the Hornsund fjord (Fig. 1), in the vicinity of the Stanisław Baranowski Polar Station of the University of Wrocław (77°04′20′′N, 15°11′30′′E). The first site (Profile 1) was set in the floor of the currently unglaciated valley of Bratteggdalen (Profile 1, 83 m a.s.l.). The rock floor of the Bratteggdalen is made of amphibolites and mica schist, with intercalations of metarhyolites, quartzites and laminated quartz–feldspathic rocks (Czerny et al. 1992). The topographic surface itself is made of coarse moraine deposits, reworked by periglacial processes. The latter involve solifluction of slopes and sorting on flat surfaces. The test profile is located close to the eastern shore of Myrktjørna lake, where fairly regular sorted circles have developed (Fig. 2a).

The next two sites were located on the surface of a raised marine terrace (Profiles 2 and 3, both at 10 m a.s.l). The terrace itself is a part of an extensive flight of terraces recognized along the north shore of Hornsund (Jahn 1959; Chmal 1987; Karczewski et al. 1990). Solid bedrock of raised marine terraces at the test sites is built of white and green quartzites of the Gulliksenfjellet formation (Czerny et al. 1992). Profile 2 runs across large non-sorted polygons in fine angular debris cover (Fig. 2b). Profile 3 is located on the surface covered by well-sorted beach material in gravel fraction, mostly 5–15 cm in diameter. Spaces between gravel are filled by finer mineral-organic deposits. These form regular non-sorted nets of low ground convexities (Fig. 2c). Terrace surfaces are subject to initial soil-forming processes and the local soils are classified as cryosols and regosols (Kabała & Zapart 2009; Szymański et al. 2013; Migała et al. 2014), with a significant content of pebbles, sandy or sandy loam texture, and volumetric soil water content locally exceeded 50%.

Climatic conditions in the study area are well known on account of long-term monitoring carried out at the permanent research base of the Polish Academy of Sciences in Hornsund, ca. 15 km to the south-east. The mean annual temperature for the 1979–2009 interval was −4.3°C, while periods with a mean temperature above 0°C occur in May/June and September/October (Marsz 2013a). Somewhat different topoclimatic conditions typify the valley Bratteggdalen, where warming due to foehn winds is occasionally noted (Pereyma 1988). Air humidity is high, being 79.4% on average and even higher in the summer months (Marsz 2013b). Annual precipitation is 434.4 mm on average, with monthly maximum values during monitoring period peaking in August (64.4 mm; Łupikasza 2013).

In the context of patterned ground formation data of ground, thermal characteristics are relevant. In Hornsund, snow cover persists for 244 days in a year on average (Niedźwiedź & Styszyńska 2013). Permafrost thickness in mountain valleys and under the strandflat has reached ca. 100 m, diminishing towards the coastline (Humlum et al. 2003; Harris et al. 2009). Recent electrical resistivity measurements showed that permafrost is discontinuous along the shoreline (Kasprzak & Kondracka 2013).

Citation: *Polar Research* 2015, *34*, 25678, http://dx.doi.org/10.3402/polar.v34.25678

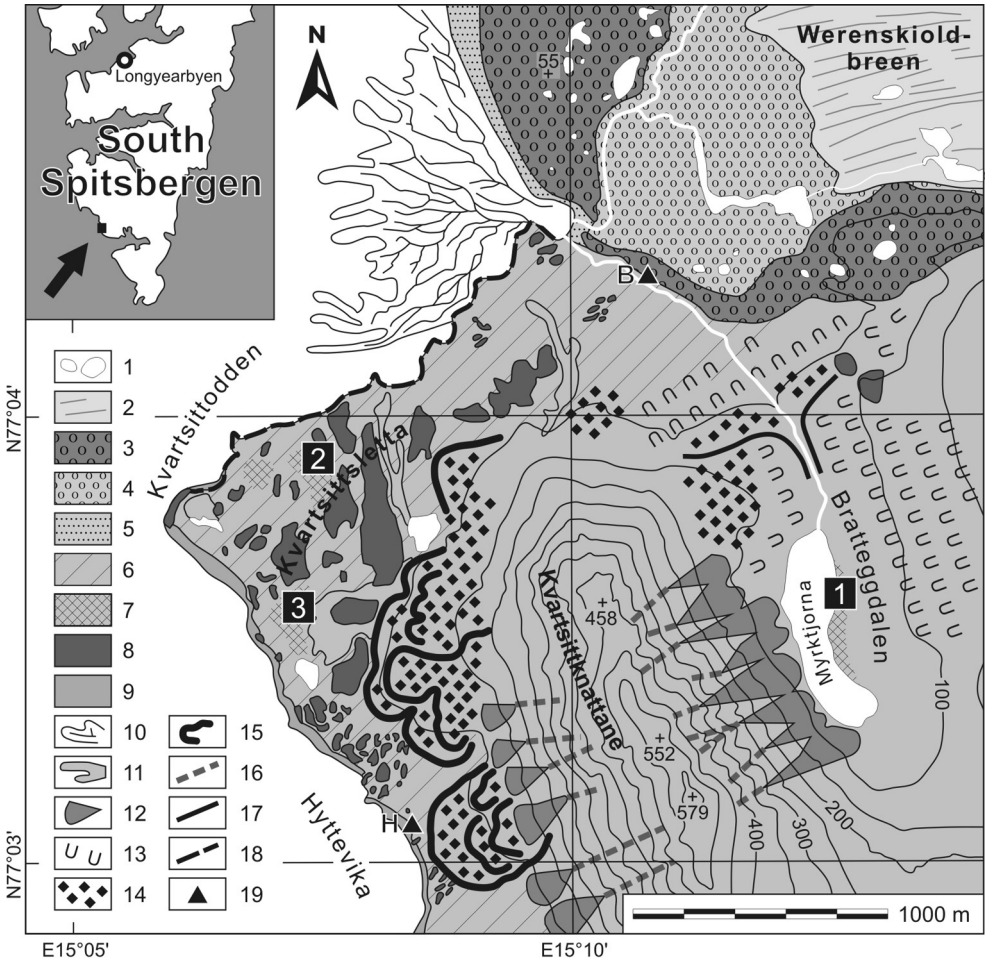

Fig. 1 Study area: water bodies (1), glacier (2), terminal and lateral moraine (3), ground moraine and inner outwash plain on bedrock or dead ice (4), outer outwash plain (5), raised marine terraces (6), main areas of patterned ground occurrence (7), rock outcrops, including relict sea cliffs (8), beach (9), delta sediments in the Nottinghambukta bay (10), pronival fan (11), debris cones (12), solifluction lobes (13), block covers (14), rock glacier faces (15), chutes (16), rock ridge (17), active sea cliffs (18), cabins (19), Stanisław Baranowski Polar Station (B), Hyttevika House (H).

A number of researchers observed and measured seasonal thawing of the active layer in the Hornsund area (Baranowski 1968; Jahn 1982; Grześ 1985; Migała 1994; Leszkiewicz & Caputa 2004). Depending on local relief and the type of substrate, its thickness is 100–115 cm on average. Very moist loams under vegetated surfaces of raised marine terraces thaw to the average depth of 70 cm, while the thickness of the active layer in waterlogged hollows filled with mud may approach 90 cm. A greater depth of summer thaw was recorded beneath large polygons (down to 140 cm) and stone circles (also 140 cm). Jahn (1948) maintained that coarse materials with numerous voids between the stones may play the role of canals supplying warm air into the ground. An even greater thickness of the active layer was reported from marine gravel and sands, reaching as much as 138–221 cm (Migała 1994) or 230 cm (Chmal et al. 1988). On outwash fans, the active layer is typically 100–110 cm thick, whereas on ice-cored moraines its thickness varies from 30 to 175 cm. Summer thaw is least efficient on turf- and peat-covered surfaces, where the active layer is ca. 40 cm thick (Jahn 1982).

During systematic measurements carried out by Czeppe (1961) on sorted circles in the Hornsund area in 1957–58, more than 120 days with temperatures above 0°C in the near-ground air layer were recorded in one year. Sometimes, a few freeze–thaw cycles occurred in one day. Daily amplitudes were very high in summer, well exceeding 10°C, while the highest soil surface temperature measured between June 24 and September 9 of 2008 was 22°C (Migała et al. 2014). A characteristic feature of the local thermal regime is a sharp transition from low temperatures and high amplitudes in winter to higher temperatures and lower amplitudes in spring.

Fig. 2 (a) Profile 1 across sorted circles in the Brattegdallen valley. (b) Profile 2 on non-sorted polygons on a 10 m high raised marine terrace. (c) Profile 3 on the net with sorted coarser material on a 10 m high raised marine terrace. (d) Well-developed sorted circles in the Hornsund fjord, measured by Czeppe (1961) with the Bac movement detector half a century ago. Probably photographed for the first time in 1957, they were presented by Jahn (1975) and Washburn (1979). (Photos by M. Kasprzak.)

Citation: *Polar Research* 2015, *34,* 25678, http://dx.doi.org/10.3402/polar.v34.25678

The same annual course of temperatures is observed at the depth of 5 cm in the ground (Czeppe 1961). In the near-surface layer, a few centimetres thick, two periods of cyclic oscillations around 0°C may be identified, in spring and autumn, respectively. In the lower part of the active layer, the spring period is not detectable; freeze–thaw oscillations are recorded in autumn only. Baranowski (1968) undertook ground temperature measurements from 1 October 1957 to 24 August 1958 and noticed that while 80 cycles with double crossing of 0°C temperature occurred at the height of 50–100 cm above ground and 50 cycles occurred at the ground surface, the respective numbers at depths of 10 and 50–160 cm were only 13 cycles and 1 cycle, respectively.

Czeppe (1961) used the Bac movement detectors on well-developed sorted stone circles in the Hornsund area (Fig. 2d) and observed five main phases of ground movement in an annual rhythm. These were: (i) repetitive heave and sinking of surface layer from August till the end of October; (ii) permanent, although non-steady soil heave from early November to early January; (iii) ultimate ground freezing and minor movements beneath snow cover during winter; (iv) disappearance of snow cover and ground subsidence from early spring to mid-April; and (v) rapid thawing after snow cover is gone and further ground subsidence. Vertical displacements of stone circles were much weaker than displacements of fine soil fraction. No evidence of circulation currents was found (i.e., no tilt of rods in the movement detectors).

Methods

To discern the internal structure of the patterned ground, ERT was employed as a method widely used in non-invasive ground investigation (e.g., Samouëlian et al. 2005; Schrott & Sass 2008; Van Dam 2012; Loke et al. 2013). In electrical resistivity surveying, resistance (R) is measured in many four-electrode arrays. Electric current (I) is passed into the ground through two electrodes (C1, C2), while the voltage (i.e., potential difference—V) is measured by another pair of electrodes (P1, P2). Since the ground material is not homogeneous, the measured resistance, expressed as a ratio of voltage to current intensity multiplied by the k coefficient dependent on the electrode array, is in fact an apparent resistivity. Moving measurements along a profile and increasing the spacing between the electrodes (electrode spacing is proportional to survey depth) yield many measurement points arranged in separate horizons. This kind of electrical imaging brings together advantages of sounding and traversing. The method is suitable for discerning forms and structures associated with the presence of permafrost and various types of ground ice and finds an increasing number of applications (Krautblatter & Hauck 2007; Kneisel et al. 2008; Harris et al. 2009; Hilbich et al. 2009; Lewkowicz et al. 2011; Watanabe et al. 2012; Kneisel et al. 2014). Its increasing popularity is also related to recent developments in software used in data processing, designed to operate in an automatic manner, with minimal inputs from the user (Griffiths & Barker 1993; Loke 2000, 2013a, b).

Measurement sites were selected following an assumption of relatively low electrical resistivity of the ground. The profiles were, therefore, placed across sufficiently moist patterned ground localities. At the same time, these are the best developed examples of sorted circles, non-sorted polygons and non-sorted stone stripes, which occur in the vicinity (ca. 10 km) of the Stanisław Baranowski Polar Station.

Fieldwork was carried out on 27–31 July 2012. Geophysical measurements were performed using ARES equipment (GF Instruments, Brno, Czech Republic). To obtain data which would be most accurate in the horizontal pattern and to limit vulnerability to inductive noise, the dipole–dipole electrode array was used (Loke 2000; Milsom 2003); for comparative purposes, the Wenner–Schlumberger array was also tried. Electrodes were inserted into the ground closely together, at 0.3 or 0.8 m intervals, resulting in a very dense network of measurement points. The distances between the end electrodes in particular profiles were 11.7 m (Profiles 1 and 3) and 31.2 m (Profile 2).

The raw results of the ground electrical resistivity measurements, expressed in Ω m, were processed using the standard procedure of inversion using RES2DINV software (Geotomo Software, Gelugor, Malaysia) and employing the default smoothness-constrained inversion formula (least-squares inversion, initial Damping factor 0.160, minimum Damping factor 0.015). Processing of this sort is applied to show the distribution of electrical resistivity values along a profile. Resulting models of this L1-norm inversion scheme were compared to models obtained from the L2-norm (robust) inversion method because the robust method reduced the effects of "outlier" data points where the noise comes from errors or equipment problems (Loke 2013a). Prior to that, data points with obviously incorrect resistivity values were eliminated. These errors were likely caused by technical problems during measurements, such as poor contact of certain electrodes with the ground. To enhance the credibility of the results, the distribution of the percentage difference between the logarithms of the observed and calculated apparent resistivity values was analysed, and the points with large errors (above 100% in root mean square error

statistics) were removed (Loke 2013a). Iterative modelling techniques produced electrical tomograms of materials beneath the ground surface. Topography along the profiles was incorporated into inversion model using distorted finite-element grid (distortion damping factor 0.75), where an effect of the topography is reduced with depth. For graphic visualization of the inverse results, logarithmic contour intervals were used. To facilitate direct visual comparisons, the three output tomograms were compiled using a common colour scale. Additionally, raw data (apparent resistivity pseudosections) are shown (Fig. 3) to facilitate interpretation of results.

Because of constraints discussed earlier, none of the profiles was excavated in a trench. Hence, geological–geomorphological interpretation of the tomograms could have been only supported by observations of surface structures and by analogies to the rather limited number of outcrops presented elsewhere in the literature (e.g., Washburn 1969; Schunke 1975). Reference resistivity values of various bedrock materials available in the literature (Stenzel & Szymanko 1973; Telford et al. 1990; Reynolds 1997; Kearey et al. 2002; Kneisel & Hauck 2008) were of limited assistance, since the value ranges for particular types of subsurface materials are very wide and often overlap one another (Table 1). The final results were certainly influenced by factors which are difficult to separate, such as structural and textural features of sediments, mineralogical composition, salinity, water content and its mineralization, freezing of the bottom parts of the profiles and the presence of air-filled voids in the near-surface coarse materials.

Results and interpretation

Profile 1: stone circles

Profile 1 runs across two regular stone circles of ca. 4 m in diameter (Fig. 2a). Their outer parts are developed as raised rings 30 cm high, built of angular debris 10–30 cm long (occasionally boulders up to 50 cm long). Inside the circles, there occurs fine-grained material (small debris, sand, silt and clay) that shows strong thixotropic soil behaviour, especially in the middle parts of the most moist polygons at the Myrktjørna lake shore. Here, the solid ground surface started to behave as a viscous fluid after disturbance (hitting).

In the profile, the minimal spacing between active electrodes was 0.3 m, and the maximal length was 11.7 m. The measured apparent resistivity values varied from 0.019 to 100 kΩ m. The measured apparent resistivity pseudosection shown as a miniature in Fig. 3a indicates evident inhomogeneities of the ground, both at the near-surface level and in deeper horizons. Raw data pseudosection shows the highest values in deep parts of the profile, with the points of lowest apparent resistivity located closer to the surface at centres of stones circles. Missing data in the pseudosections images are the result of automatic switching off of those electrodes, which registered poor grounding and to low measuring current. The inversion results for the electrical imaging show considerable differentiation of geoelectrical properties across the stone circles (Fig. 3a). The minimal resistivity values (<50 Ω m) typify the inner parts of the circles and may be related to high moisture content and little volume of soil air. Similarly, low values are characteristic for the horizons beneath the debris rings. By contrast, the near-surface bodies of coarse debris with large voids have the highest values of resistivity ($\rho > 2$ kΩ m), which seems to be a joint effect of ground electrical properties and the presence of air. The resistivity of deeper ground is high too and may be linked with its frozen state. The tomogram clearly returns the wavy permafrost table at the depth of 0.5–1 m, mimicked by the surface pattern of sorted structures and the geoelectrical properties of the near-surface materials.

Profile 2: non-sorted polygons

Profile 2 was placed across the network of cracks delineating large polygons (7–14 m across; some polygons in the vicinity are larger), mainly hexagonal in shape (Fig. 2b). At the surface, there occurs fine angular debris with finer fractions, mixed with organic material. Sporadic larger debris elements are present in the middle of the polygons. The debris material conceals the solid quartzite bedrock, developed as an abrasion platform of the raised marine terrace. The topographic surface is gently inclined towards the sea (ca. 3°), in the direction consistent with that of the profile.

The minimal spacing between active electrodes in this profile was 0.8 m, while the maximum length was 31.2 m. The central part of the profile runs above two distinct polygons. The electrode spacing, larger than in the two other examples, was dictated by the size of the sorted landforms. The measured values of apparent resistivity varied from 2.1 to 13.2 kΩ m.

The model obtained from the inversion procedure is clearly bipartite (Fig. 3b). Its upper part, ca. 2 m thick and of lower resistivity in general, is more heterogeneous in terms of geoelectrical properties. It may be interpreted as the thawed active layer. It is not unlikely that its bottom is made of solid bedrock, as suggested by fairly

Citation: *Polar Research* 2015, *34*, 25678, http://dx.doi.org/10.3402/polar.v34.25678

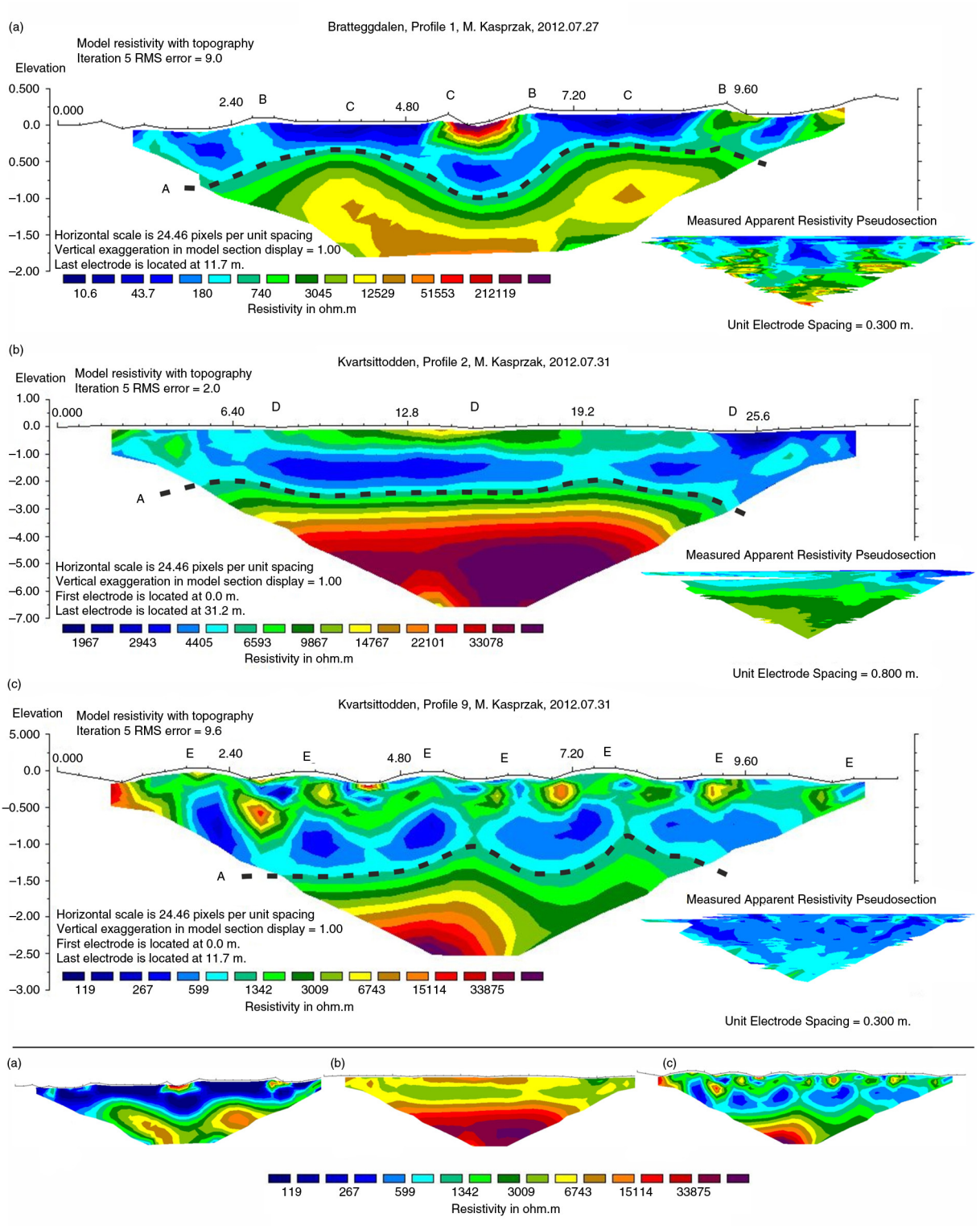

Fig. 3 Inversion results of electrical imaging across (a) sorted circles, (b) non-sorted polygons and (c) sorted net with coarser material. The locations of features are indicated as follows: permafrost table (A), crests of debris rings (B), fine material inside the circles (C), cracks (D) and gravel mounds (E).

Table 1 Range of resistivity for different materials. Compilation based on Stenzel and Szymanko (1973), Telford et al. (1990), Reynolds (1997), Kearey et al. (2002) and Kneisel & Hauck (2008).

Material	Range of resistivity (Ω m)
Clay	$1–10^2$
Sand	$10^2–5 \times 10^3$
Gravel	$10^2–4 \times 10^2$
Saturated sands and gravels	$8 \times 10–3.5 \times 10^2$
Moraine	$10–5 \times 10^3$
Crystalline rocks, extrusive and metamorphic (gneiss type)	$>10^3$
Quartzite	$10–10^9$
Schist	$10^2–10^4$
Natural waters (sediments)	$1–10^2$ (average: 3)
Surface waters (sediments)	$10–10^2$
Groundwaters	$10–3 \times 10^2$
Acid peat waters	10^2
Rainfall runoff	$2 \times 10–10^2$
Frozen sediments, ground ice, permafrost	$10^3–10^6$
Air	Infinity

high resistivity values (ca. 2–6 kΩ m). The near-surface horizons of the upper layer, represented by debris material, have an elevated resistivity and these are correlated with convex polygon surfaces. Next to the cracks, the resistivity decreases and reaches values, which are the lowest in the entire profile (2 kΩ m), although the crack in the middle sector of the profile does not show this behaviour. The presence of very low values close to the topographic surface may be directly linked with the occurrence of wet ground hollows (the crack in the centre is not in the least elevated part of the profile). Clear vertical structures with specific geoelectrical signatures were not recorded. The lower part of the profile, from 2 to 2.5 m depth downward, is likely frozen throughout, as suggested by very high values of calculated electric resistivity (6–35 kΩ m and more). Its upper boundary, interpreted as the permafrost table, is fairly uniform in shape and indistinctly plunges towards the end of the profile. This zone coincides with the termination of the area occupied by regular polygons as seen at the surface.

Profile 3: polygonal net with sorted coarser material

Profile 3 runs across beach deposits of a raised marine terrace, composed mainly of quartzite pebbles 5–20 cm in diameter, with an admixture of finer fraction (Fig. 2c). Convex stripes of pebbles, up to 1 m wide, are locally replaced by rows of isolated hummocks. The terrain depressions between the hummocks are moist and overgrown by moss and other vegetation. Elevation differences within the profile do not exceed 30 cm. The surface of the raised terrace occupied by this patterned ground is surrounded by the rock-cut landforms indicative of past wave action (relict cliffs and skjerries).

In the profile, which runs across eight parallel stone stripes, the minimal spacing between active electrodes was 0.3 m, while the maximum distance was 11.7 m. The measured values of apparent resistivity varied from 0.096 to 7.9 kΩ m.

The resultant inversion model indicates considerable geoelectrical diversity of the profile (Fig. 3c). The lower part, with very high resistivity ($\rho > 1$ kΩ m), can be safely interpreted as frozen ground. The permafrost table, as in profile 1, is wavy but occurs at greater depth, 1–1.5 m below the topographic surface. Its shape is mirrored by low resistivity ($\rho < 0.8$ kΩ m) cells immediately above. Higher up, next to the surface, one can see alternating cells of higher ($\rho > 0.8$ kΩ m) and lower ($\rho < 0.8$ kΩ m) resistivity, which also relate to the geoelectrical pattern identified below. It cannot be ruled out that the highest values in this layer are associated with individual large cobbles, while the lowest ones typify ground portions built of fine fraction with high water content.

Discussion

Measurements of apparent resistivity and the interpretation of inversion models are sensitive to various types of errors, which need to be realized before drawing definitive conclusions. For instance, spacing between the electrodes inserted into the ground exhibiting some surface microrelief may not have been identical in each case, despite special care involved. Therefore, the inversion procedure may have suffered from errors whose magnitude increased towards the topographic surface (for the nearest active electrodes).

Errors may also have resulted from insufficient contact of electrodes with the ground materials. This was undoubtedly the case in Profile 1, where single electrodes in loose debris on the stone circles were automatically ignored in the measurement because of anomalously high resistivity ($\rho > 20$ kΩ m) shown during a test trial. In consequence, a large root mean square error—indicating a large difference between values predicted by the model and the values observed—was noted. However, this complication was unavoidable since it was decided not to artificially improve electrical conductivity in the vicinity of loosely fitted electrodes. The choice of the measurement and inversion methods (with different numbers of iterations) has certainly influenced the results, too (Fig. 4). The application of the dipole–dipole electrode array allowed us to obtain very detailed electrical imaging, with a large number of measuring points (Fig. 4a–c), but

Citation: *Polar Research* 2015, *34*, 25678, http://dx.doi.org/10.3402/polar.v34.25678

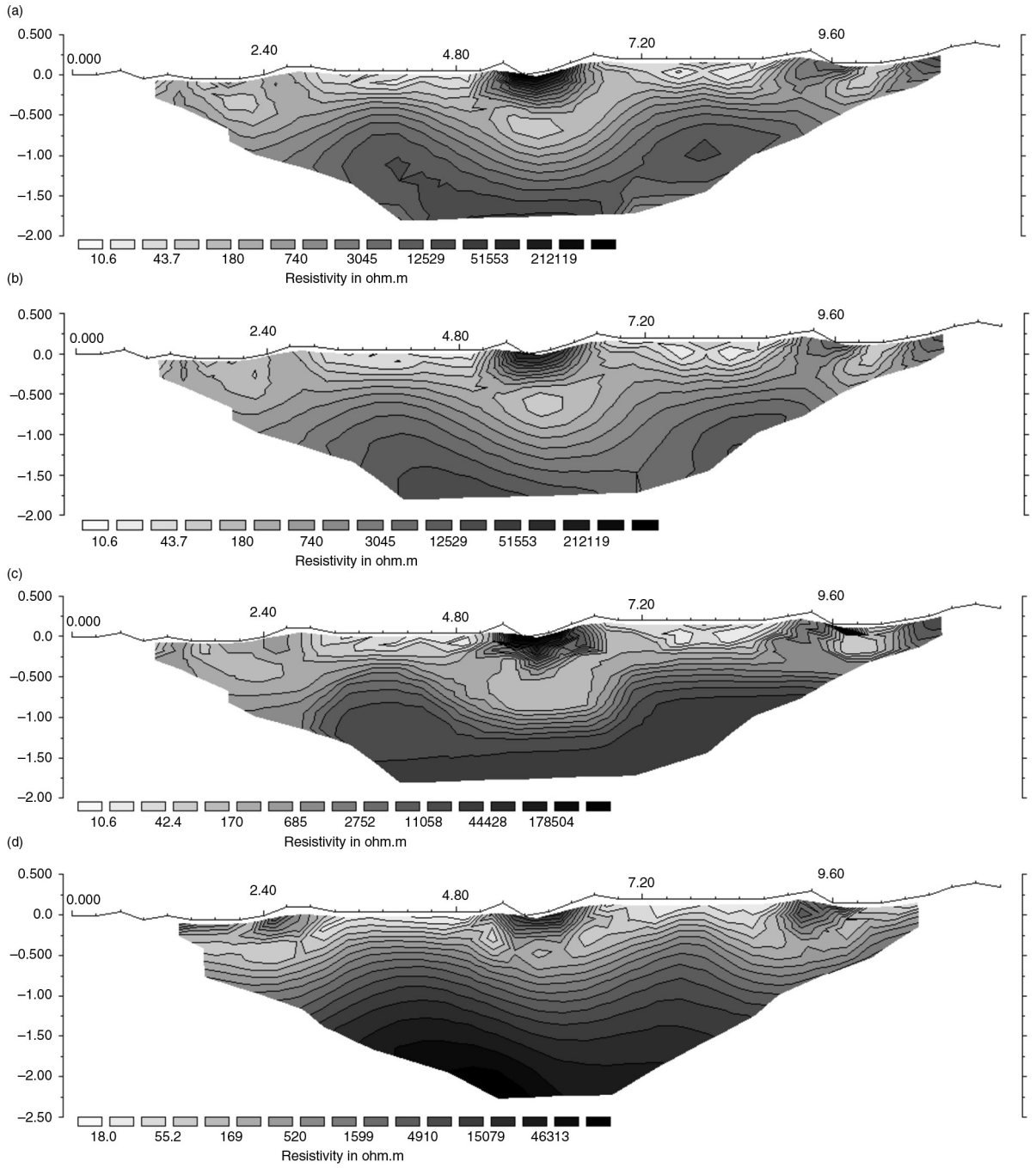

Fig. 4 The comparison of conventional least-squares inversion method from imaging using the dipole–dipole electrode array: (a) after five iterations, (b) after three iterations and (c) from robust inversion method. For comparison, imaging from the Wenner–Schlumberger electrode array is shown in (d).

the differences between the results from this array and those from the Wenner–Schlumberger array (Fig. 4d) are evident. In the latter, the measured apparent resistivity values varied from 0.017 to 11.7 kΩ m—an order of magnitude less for the maximum values compared to those from the dipole–dipole array, although the set of values in both tomography are within the same order of magnitude (ρ quartiles $Q_1 = 98.66$, $Me = 201.51$, $Q_3 = 433.01$ Ω m for Wenner–Schlumberger and. $Q_1 = 36.10$, $Me = 143.29$, $Q_3 = 692.22$ Ω m for dipole–dipole).

The inversion model from the Wenner–Schlumberger method shows different resistivity below each crest of debris ridge than that from dipole–dipole method. These differences may have resulted from a dissimilar spatial extent of measurement points defined by various geometries of the measurement patterns. The inversion model derived from the Wenner–Schlumberger array and data is less detailed, but the adverse effects of low/high values along the image borders on the interpolation procedure are also smaller. A related problem in the construction of tomograms is exemplified in Fig. 3, particularly Profiles 1 and 2. The interpolation procedure effectively excludes the lower ends of the tomograms from any interpretation. The L1-norm (robust) inversion scheme produced models with sharper interfaces between parts with different resistivity values with more constant resistivity in each of the imaged regions (Fig. 4c). This is a consequence of this inversion scheme attempting to minimize the absolute changes in the resistivity values (Loke 2013a).

The interpretation itself, in the absence of test trenches or pits, cannot be deemed entirely accurate and in practice it is restricted to the recognition of general characteristics of conductivity/resistivity in different parts of the profiles. Given that resistivity depends on many factors, inferences about the actual geological situation underground have to be based on surface observations, analogies to other test sites, including outcrops and operator's experience. It is emphasized that boundaries between materials typified by different values of electrical resistivity should not be directly related to the variability of one specific lithological feature.

Despite these problems and uncertainties, the inversion results for the test profiles show that the method adopted in this study suits the purpose of the research well and can be used for non-invasive investigation of patterned ground, providing the physical environment of the study area allows for measurements to be carried out (i.e., moist regolith). It is further asserted that the ERT, if compared with other geophysical techniques (Kneisel et al. 2008; Harris et al. 2009), yields results which are easier to interpret. However, to achieve comparable data sets, electrodes must be very closely spaced. Such an approach has been used to date in weathering studies of rock walls (Mol & Viles 2010) and building stone deterioration (Saas & Viles 2010), and also in engineering testing of concrete (Karhunen 2013). The use of the method for dry debris materials, with large air-filled voids, is considerably more difficult.

The results of this study show that as far as geoelectrical properties of the sediments are concerned, the ground structure at the study sites is likely more complex than suggested by grain-size characteristics alone and simple conceptual cross-sections of patterned ground available in the literature. This is evident in Profile 3, where the inversion model reveals cells typified by diverse geoelectrical features, arranged in separate horizons, parallel to one another and to the permafrost table. The resultant electrical resistivity image bears similarities to the hexagonal Rayleigh convection cells in the active layer, as presented by Ray et al. (1983) and Krantz (1990). In the model proposed by these authors, the regular pattern of the polygons is an outcome of pore water convection driven by temperature gradients in the active layer.

Although ERT cannot mimic the real subsurface, it could be helpful in determining the active layer depth and the shape of the permafrost table. In the given examples, the thickness of the active layer may be interpreted to be 0.5–1 m in the mountain valley and 1–2.5 m beneath the surface of raised marine terraces, which generally coincides with the observations of other authors (Baranowski 1968; Jahn 1982; Grześ 1985; Chmal et al. 1988; Migała 1994). The evident mimicking the shape of the permafrost table by the geometry of sorted stone circles (or vice versa), as seen in Profile 1, has been noted by several previous authors. However, the relationship was presented in an opposite way, i.e., depressions of the permafrost table were located under the central parts of the structures (e.g., Troll 1958; Hallet & Prestrud 1986; Kling 1997; Hallet 2013). Other authors did not imply such a relationship (Jahn 1975; Tedrow 1977). By contrast, Smith (1956) offered a view very consistent with the one recognized in Profile 1, based on observations in the southern part of Isfjorden in Spitsbergen. The lowering of the permafrost table was not identified in Profile 2, across non-sorted polygons. It is therefore proposed that the lack of sorting is genetically connected with the permafrost table, or vice versa, but this conclusion is only tentative due to the limited number of test sites. Additionally, no literature citations indicate such a large amplitude (ca. 0.5 m) of wavy permafrost table below non-sorted polygons. The lack of a wavy permafrost table beneath these non-sorted polygons in the tomogram might be an effect of smoothing in the process of iteration and imaging. This should be resolved by further research and measurements of temperature in the ground.

Conclusion

Closely spacing electrodes in 2-D ERT reveals subtle differences in resistivity in different sources of patterned ground and allows for inferences regarding the position and shape of the permafrost table. However, different

Citation: *Polar Research* 2015, *34*, 25678, http://dx.doi.org/10.3402/polar.v34.25678

types of errors are inherent to the method, such as those related to uneven spacing of electrodes. Interpretation of inversion results is based on resistivity properties of ground materials, which in turn reflect a range of lithological features such as mineral composition, density, structure and texture of the deposit, water content, including its temperature and mineralization, as well as the presence of ice and air.

This study has shown how, in the investigation of sorted stone circles, ERT indicates a direct relationship between the wavy surface of the permafrost table, internal ground structure and the geometric pattern on the surface exists. The pattern obtained in this study is unlike those often presented in the literature. In the investigation of non-sorted polygons, little variability of the permafrost table was detected. No vertical structures in the ground were resolved in the tomogram. In the net with sorted coarser materials, the shape of the permafrost table was closely followed by the complicated geoelectrical structure of the sediment above it. Geometries of individual isolated cells may be related to convective processes that could be responsible for the differentiation of this patterned ground.

Acknowledgements

The author is grateful to the Rector of the University of Wrocław and the Director of the Institute of Geography and Regional Development of the University of Wrocław for financial support, which enabled the organization of the XXV Polar Expedition of the University of Wrocław to Spitsbergen. The assistance of Mr Krzysztof Senderak during fieldwork is gratefully acknowledged. Corrections and suggestions from journal reviewers proved most helpful in revising the first version of the paper.

References

Ballantyne C.K. 2007. Patterned ground. In A.E. Scott (ed.): *Encyclopedia of quaternary science*. Pp. 2182–2191. Amsterdam: Elsevier.

Ballantyne C.K. & Matthews J. 1982. The development of sorted circles on recently deglaciated terrain, Jotunheimen, Norway. *Arctic and Alpine Research 14*, 341–354.

Ballantyne C.K. & Matthews J. 1983. Desiccation cracking and sorted polygon development, Jotunheimen, Norway. *Arctic Alpine Research 15*, 339–349.

Baranowski S. 1968. *Termika tundry peryglacjalnej SW Spitsbergen. (Thermic conditions of the periglacial tundra in SW Spitsbergen.) Polish I.G.Y. and I.G.C. Spitsbergen Expeditions in 1957–1960. Studia Geograficzne 10, Acta Universitatis Wratislaviensis 68*. Wrocław: University of Wrocław.

Boardman J. (ed.) 1987. *Periglacial processes and landforms in Britain and Ireland*. Cambridge: Cambridge University Press.

Chmal H. 1987. Pleistocene sea level changes and glacial history of the Hornsund area, Svalbard. *Polar Research 5*, 269–270.

Chmal H., Klementowski J. & Migała K. 1988. Thermal currents of active layer in Hornsund area. Permafrost. In K. Senneset (ed.): *Proceedings of the Fifth International Conference on Permafrost, Trondheim, June 1988. Vol. 1*. Pp. 44–49. Trondheim: Tapir.

Christensen L. 1974. Crop-marks revealing large-scale patterned ground structures in cultivated areas, southwestern Jutland, Denmark. *Boreas 3*, 153–180.

Czeppe Z. 1961. *Roczny przebieg mrozowych ruchów gruntu w Hornsundzie (Spitsbergen) 1957–1958. (Annual course of frost ground movements at Hornsund [Spitsbergen] 1957–1958.) Zeszyty Naukowe Uniwersytetu Jagiellońskiego 42, Prace Geograficzne 3*. Kraków: Jagiellonian University.

Czerny J., Kieres A., Manecki M. & Rajchel J. 1992. *Geological map of the SW part of Wedel Jarlsberg Land Spitsbergen, 1:25 000*. Kraków: Institute of Geology and Mineral Deposits, University of Mining and Metallurgy.

Dąbski M. 2011. Grunty strukturalne w Polsce. (Patterned grounds in Poland.) *Przegląd Geograficzny 83*, 307–321.

Drew J.V. & Tedrow J.C.F. 1962. Arctic soil classification and patterned ground. *Arctic 15*, 109–116.

Goudie A.S. 2004. Patterned ground. In A.S. Goudie (ed.): *Encyclopedia of geomorphology. Vol. 2*. Pp. 765–766. London: Routledge.

Griffiths D.H. & Barker R.D. 1993. Two-dimensional resistivity imaging and modelling in areas of complex geology. *Journal of Applied Geophysics 29*, 211–226.

Grześ M. 1985. Warstwa czynna wieloletniej zmarzliny na zachodnich wybrzeżach Spitsbergenu. (Characteristic of permafrost active layer on the western coast of Spitsbergen.) *Przegląd Geograficzny 57*, 671–691.

Hallet B. 1998. Measurement of soil motion in sorted circles, western Spitsbergen. In A.G. Lewkowicz & M. Allard (eds.): *Proceedings of the Seventh International Conference on Permafrost, 23–27 June 1998. Collection Nordicana 57*. Pp. 415–420. Yellowknife: Centre for Northern Studies.

Hallet B. 2013. Stone circles: form and soil kinematics. *Philosophical Transactions of the Royal Society A 371*, article no. 20120357, doi: 10.1098/rsta.2012.0357.

Hallet B. & Prestrud S. 1986. Dynamics of periglacial sorted circles in western Spitsbergen. *Quaternary Research 26*, 81–89.

Harris C., Arenson L.U., Christiansen H.H., Etzelmüller B., Frauenfelder R., Gruber S., Haeberli W., Hauck C., Hölzle M., Humlum O., Isaksen K., Kääb A., Kern-Lütschg M.A., Lehning M., Matsuoka N., Murton J.B., Nötzli J., Phillips M., Ross N., Seppälä M., Springman S.M. & Mühll D.V. 2009. Permafrost and climate in Europe: monitoring and modelling thermal, geomorphological and geotechnical responses. *Earth-Science Reviews 92*, 117–171.

Hilbich C., Marescot L., Hauck C., Loke M.H. & Mäusbacher R. 2009. Applicability of electrical resistivity tomography

monitoring to coarse blocky and ice-rich permafrost landforms. *Permafrost and Periglacial Processes 20*, 269–284.

Hubbard S.S., Gangodagamage C., Dafflon B., Wainwright H., Peterson J., Gusmeroli A., Ulrich C., Wu Y., Wilson C., Rowland J., Tweedie C. & Wullschleger S.D. 2013. Quantifying and relating land-surface and subsurface variability in permafrost environments using LiDAR and surface geophysical datasets. *Hydrogeology Journal 21*, 149–169.

Humlum O., Instanes A. & Sollid J.L. 2003. Permafrost in Svalbard: a review of research history, climatic background and engineering challenges. *Polar Research 22*, 191–215.

Jahn A. 1948. *Badania nad strukturą i temperaturą gleb w Zachodniej Grenlandii. (Investigation on structure and soil temperature in West Greenland.) Rozprawy Wydziału Matematyczno-przyrodniczego 72A (1946), series III, 32(6)*. Kraków: Polish Academy of Sciences.

Jahn A. 1959. Postglacjalny rozwój wybrzeży Spitsbergenu. (Postglacial development of Spitsbergen shores.) *Czasopismo Geograficzne 30*, 245–262.

Jahn A. 1968. Patterned ground. In R.W. Fairbridge (ed.): *Encyclopedia of geomorphology*. Pp. 814–817. New York: Reinhold.

Jahn A. 1975. Patterned ground. In: *Problems of the periglacial zone (translated from Polish)*. Pp. 127–140. Warsaw: PWN Polish Scientific Publishers.

Jahn A. 1982. Soil thawing and active layer of permafrost in Spitsbergen. In: *Acta Universitatis Wratislaviensis 525, Spitsbergen Expeditions 4*. Pp. 57–75. Wrocław: University of Wrocław.

Kaatz M.R. 1959. Patterned ground in central Washington: a preliminary report. *Northwest Science 33*(*4*), 145–156.

Kabała C. & Zapart J. 2009. Recent, relic and buried soils in the forefield of Werenskiold Glacier, SW Spitsbergen. *Polish Polar Research 30*, 161–178.

Karczewski A., Andrzejewski L., Chmal H., Jania J., Kłysz P., Kostrzewski A., Lindner L., Marks L., Pękala K., Pulina M., Rudowski S., Stankowski W., Szczypek T. & Wiśniewski E. 1990. *Hornsund, Spitsbergen geomorphology, 1:75 000. (With commentary to the map by A. Karczewski.)* Katowice: Polish Academy of Sciences, Silesian University.

Karhunen K. 2013. *Electrical resistance tomography imaging of concrete. Dissertations in Forestry and Natural Sciences 122*. University of Eastern Finland, Kuopio.

Kasprzak M. & Kondracka M. 2013. Geophysical signatures of permafrost in SW Spitsbergen. In: *8th International Conference (AIG) on Geomorphology. Abstract volume. Paris—2013; 27–31 August*. P. 1042. Paris: International Association of Geomorphologists.

Kearey P., Brooks M. & Hill I. 2002. Electrical surveying. In P. Keary et al. (eds.): *An introduction to geophysical exploration*, 3rd edn. Oxford: Blackwell Science.

Kessler M.A. & Werner B.T. 2003. Self-organization of sorted patterned ground. *Science 299*, 380–383.

Kling J. 1997. Observations on sorted circle development, Abisko, northern Sweden. *Permafrost and Periglacial Processes 8*, 447–453.

Kneisel C., Emmert A. & Kästl J. 2014. Application of 3D electrical resistivity imaging for mapping frozen ground conditions exemplified by three case studies. *Geomorphology 210*, 71–82.

Kneisel C. & Hauck C. 2008. Electrical methods. In C. Hauck & C. Kneisel (eds.): *Applied geophysics in periglacial environments*. Pp. 3–27. Cambridge: Cambridge University Press.

Kneisel C., Hauck C., Fortier R. & Moorman B. 2008. Advances in geophysical methods for permafrost investigations. *Permafrost and Periglacial Processes 19*, 157–178.

Krantz W.B. 1990. Self-organization manifest as patterned ground in recurrently frozen soils. *Earth-Science Reviews 29*, 117–130.

Krautblatter M. & Hauck C. 2007. Electrical resistivity tomography monitoring of permafrost in solid rock walls. *Journal of Geophysical Research—Earth Surface 112*, F02S20, doi: 10.1029/2006JF000546.

Leszkiewicz J. & Caputa Z. 2004. The thermal condition of the active layer in the permafrost at Hornsund, Spitsbergen. *Polish Polar Research 25*, 223–239.

Lewkowicz A.G., Etzelmüller B. & Smith S.L. 2011. Characteristics of discontinuous permafrost based on ground temperature measurements and electrical resistivity tomography, southern Yukon, Canada. *Permafrost and Periglacial Processes 22*, 320–342.

Loke M.H. 2000. *Electrical imaging surveys for environmental and engineering studies. A practical guide to 2-D and 3-D surveys*. Gelugor, Malaysia: Geotomo Software.

Loke M.H. 2013a. *Rapid 3-D resistivity & IP inversion using the least-squares method (for 3-D surveys using the pole–pole, pole–dipole, dipole–dipole, rectangular, Wenner, Wenner–Schlumberger and non-conventional arrays). On land, aquatic and cross-borehole surveys*. Gelugor, Malaysia: Geotomo Software.

Loke M.H. 2013b. *Tutorial: 2-D and 3-D electrical imaging surveys*. Gelugor, Malaysia: Geotomo Software.

Loke M.H., Chambers J.E., Rucker D.F., Kuras O. & Wilkinson P.B. 2013. Recent developments in the direct-current geoelectrical imaging method. *Journal of Applied Geophysics 95*, 135–156.

Łupikasza E. 2013. Atmospheric precipitation. In A.A. Marsz & A. Styszyńska (eds.): *Climate and climate change at Hornsund, Svalbard*. Pp. 199–211. Gdynia, Poland: Gdynia Maritime University.

Lusch D.P., Stanley K.E., Schaetzl R.J., Kendall A.D., Van Dam R.L., Nielsen A., Blumer B.E., Hobbs T.C., Archer J.K., Holmstadt J.L.F. & May C.L. 2009. Characterization and mapping of patterned ground in the Saginaw Lowlands, Michigan: possible evidence for Late-Wisconsin permafrost. *Annals of the Association of American Geographers 99*(*3*), 1–22.

Milsom J. 2003. *Field geophysics.* 3rd edn. Chichester: Wiley.

Marsz A.A. 2013a. Air temperature. In A.A. Marsz & A. Styszyńska (eds.): *Climate and climate change at Hornsund, Svalbard*. Pp. 145–187. Gdynia, Poland: Gdynia Maritime University.

Marsz A.A. 2013b. Humidity. In A.A. Marsz & A. Styszyńska (eds.): *Climate and climate change at Hornsund, Svalbard*. Pp. 189–198. Gdynia, Poland: Gdynia Maritime University.

Matsuoka N., Abe M. & Ijiri M. 2003. Differential frost heave and sorted patterned ground: field measurements and a laboratory experiment. *Geomorphology 52*, 73–85.

Migała K. 1994. Cechy warstwy aktywnej wieloletniej zmarzliny w warunkach klimatycznych Spitsbergenu. (The characteristic features of the active layer of the permafrost in the climate of Spitsbergen.) In L. Pyka (ed.): *Klimat Dolnego Śląska i krain polarnych. (Climate of Lower Silesia and polar lands.) Acta Universitatis Wratislaviensis 1590. Prace Instytutu Geograficznego C Meteorologia i Klimatologia 1*. Pp. 79–111. Wrocław: University of Wrocław.

Migała K., Wojtuń B., Szymański W. & Muskała P. 2014. Soil moisture and temperature variation under different types of tundra vegetation during the growing season: a case study from the Fuglebekken catchment, SW Spitsbergen. *Catena 116*, 10–18.

Mol L. & Viles H.A. 2010. Geoelectric investigations into sandstone moisture regimes: implications for rock weathering and the deterioration of San rock art in the Golden Gate Reserve, South Africa. *Geomorphology 118*, 280–287.

Niedźwiedź T. & Styszyńska A. 2013. Snow cover at the Hornsund Station. In A.A. Marsz & A. Styszyńska (eds.): *Climate and climate change at Hornsund, Svalbard*. Pp. 367–372. Gdynia, Poland: Gdynia Maritime University.

Overduin P.P. & Kane D.L. 2006. Frost boils and soil ice content: field observations. *Permafrost and Periglacial Processes 17*, 291–307.

Pereyma J. 1988. Climatology. In R. Brázdil et al. (eds.): *Results of investigations of the geographical research expedition Spitsbergen 1985*. Pp. 55–68. Brno, Czech Republic: Jan Evangelista Purkyne University.

Peterson R.A. & Krantz W.B. 2008. Differential frost heave model for patterned ground formation: corroboration with observations along a North American Arctic transect. *Journal of Geophysical Research—Biogeosciences 113*, G03S04, doi: 10.1029/2007JG000559.

Ray R.J., Krantz W.B., Caine T.N. & Gunn R.D. 1983. A model for sorted patterned-ground regularity. *Journal of Glaciology 29*, 317–337.

Reynolds J.M. 1997. *An introduction to applied and environmental geophysics*. Chichester: Wiley.

Saas O. & Viles H.A. 2010. Wetting and drying of masonry walls: 2D-resistivity monitoring of driving rain experiments on historic stonework in Oxford, UK. *Journal of Applied Geophysics 70*, 72–83.

Samouëlian A., Cousina I., Tabbagh A., Bruandd A. & Richard G. 2005. Electrical resistivity survey in soil science: a review. *Soil and Tillage Research 83*, 173–193.

Schaetzl R. & Anderson S. 2005. *Soil genesis and geomorphology*. Cambridge: Cambridge University Press.

Schrott L. & Sass S. 2008. Application of field geophysics in geomorphology: advances and limitations exemplified by case studies. *Geomorphology 93*, 55–73.

Schunke E. 1975. Neue Beobachtungen zur Periglacialmorphologie Islands (Ein Forschungsbericht). (New observations to periglacial morphology of Iceland [research report].) *Die Erde, Zeitschrift der Gesellschaft für Erdkunde zu Berlin 106*, 47–56.

Sekyra J. 1956. The development of cryopedology in Czechoslovakia. *Biuletyn Peryglacjalny 4*, 351–369.

Smith J. 1956. Some moving soils in Spitsbergen. *Journal of Soil Science 7*, 11–21.

Stenzel P. & Szymanko J. 1973. *Metody geofizyczne w badaniach hydrogeologicznych i geologiczno-inzynierskich. (Geophysical methods in hydrogeological and engineering-geological studies.)* Warsaw: Geological Publishers.

Szymański W., Skiba S. & Wojtuń B. 2013. Distribution, genesis, and properties of Arctic soils: a case study from the Fuglebekken catchment, Spitsbergen. *Polish Polar Research 34*, 289–304.

Tedrow J.C.F. 1962. Morphological evidence of frost action in Arctic soils. *Biuletyn Peryglacjalny 11*, 343–352.

Tedrow J.C.F. 1977. *Soils of the polar landscapes*. New Brunswick, NJ: Rutgers University Press.

Telford W.M., Geldart L.P. & Sheriff R.E. 1990. *Applied geophysics*. 2nd edn. Cambridge: Cambridge University Press.

Troll C. 1958. *Structure soils, solifluction, and frost climates of the Earth. Translation 43*. Wilmette, IL: US Army Snow, Ice and Permafrost Research Establishment, Corps of Engineers.

Van Dam R.L. 2012. Landform characterization using geophysics—recent advances, applications, and emerging tools. *Geomorphology 137*, 57–73.

van Everdingen R.O. 2005. *Multi-language glossary of permafrost and related ground-ice terms*. Boulder, CO: National Snow and Ice Data Centre/World Data Center for Glaciology.

Walker D.A., Epstein H.E., Gould W.A., Kelley A.M., Kade A.N., Knudson J.A., Krantz W.B., Michaelson G., Peterson R.A., Ping C.-L., Raynolds M.K., Romanovsky V.E. & Shur Y. 2004. Frost-boil ecosystems: complex interactions between landforms, soils, vegetation and climate. *Permafrost and Periglacial Processes 15*, 171–188.

Washburn A. L. 1956. Classification of patterned ground and review of suggestion origins. *Geological Society of America Bulletin 67*, 823–865.

Washburn A.L. 1969. Patterned ground in the Mesters VIG District, northeast Greenland. *Biuletyn Peryglacjalny 18*, 259–330.

Washburn A.L. 1970. An approach to a genetic classification of patterned ground. *Acta Geographica Lodziensia 24*, 437–446.

Washburn A.L. 1979. *Geocryology. A survey of periglacial processes and environments*. London: Edward Arnold.

Watanabe T., Matsuoka N. & Christiansen H.H. 2012. Mudboil and ice-wedge dynamics investigated by electrical resistivity tomography, ground temperatures and surface movements in Svalbard. *Geografiska Annaler A 94*, 445–457.

Williams R.B.G. 1964. Fossil patterned ground in eastern England. *Biuletyn Peryglacjalny 14*, 337–349.